REVIEW PAPER

Schiff Base Metal Complex Development: From Coordination Chemistry to Biological Activity: A Comprehensive Review

Mr. Jeevan Bholenath Kore*[1], Mr. Krishna S. Pathade[2], Dr. Manish S. Kondawar[3], Mr. Mahesh Tanaji Kore[4], Ms. Neha Neminath Darure[5]

[1]Research Scholer, Department of Pharmaceutical Chemistry, Appasaheb Birnale College of Pharmacy Sangli, Maharashtra, India.
[2]Assistant professor, Department of Pharmaceutical Chemistry, Appasaheb Birnale College of Pharmacy Sangli, Maharashtra, India.
[3]Professor & H.O.D. Department of Pharmaceutical Chemistry, Appasaheb Birnale College of Pharmacy Sangli, Maharashtra, India.
[4]Research Scholer, Department of Pharmaceutics, Annasaheb Dange College of B. Pharmacy Ashta, Maharashtra, India
[5]Research Scholer, Department of Pharmaceutical Chemistry, Appasaheb Birnale College of Pharmacy Sangli, Maharashtra, India.

Corresponding Author
Mr. Jeevan Bholenath Kore
Email:ID: korejb5145@gmail.com

Received: 15th March, 2026; Revised: 6th May, 2026; Accepted: 18th June, 2026; Available Online: 27th June, 2026

ABSTRACT
Schiff bases are a significant family of azomethine chemicals that are produced by condensing active carbonyl compounds with primary amines. They are extremely useful in coordination chemistry and bioinorganic research due to their capacity to coordinate with metal ions via nitrogen and oxygen donor atoms. The different synthetic techniques used to prepare Schiff base metal complexes, such as direct condensation, in situ complex formation, oxidation of coordinated secondary amines, amine exchange, metal exchange, and ligand exchange reactions, are systematically summarized in this review article. Understanding the coordination behavior and bonding mechanisms of Schiff base ligands with transition and post-transition metal ions, as documented in the literature, is emphasized. A recently synthesized Schiff base ligand, 1 [(2 {1 [(dicyclohexylamino)–methyl]–1H indol–3–yl}ethylimino)–methyl], is given particular attention.naphthalen-2-ol (HL) and its monomeric complexes with Cr(III), Fe(III), Mn(II), Cd(II), and Hg(II). Different coordination geometries, including octahedral, square planar, and tetrahedral arrangements, were confirmed by characterizing the synthesized complexes using elemental analysis, spectroscopic methods, thermal investigations, magnetic susceptibility measurements, and molar conductance analysis. The Coats-Redfern approach was used to assess kinetic parameters and thermal decomposition behavior. Density functional theory (DFT) calculations were used to examine electronic structure, spectroscopic characteristics, and electrostatic potential distribution in addition to providing support for experimental results. Additionally, a study of Schiff base complexes' antibacterial efficacy against particular bacterial and fungal species is provided, highlighting their potential as promising bioactive agents

Keywords: Schiff bases, coordination complexes, synthesis routes, DFT studies, antimicrobial activity
How to cite this article: Kore JB, Pathade KS, Kondawar MS, Kore MT, Darure NN. Schiff Base Metal Complex Development: From Coordination Chemistry to Biological Activity: A Comprehensive Review. Int J Drug Deliv Technol. 2026;16(65s):390-404. DOI: 10.25258/ijddt.16.65s.41
Source of support: Nil.
Conflict of interest: Nil.

INTRODUCTION

Schiff bases and their corresponding metal complexes have long been recognized as an important group of compounds because of their wide applicability in chemical, biological, and industrial fields[1,2]. Their importance stems from the presence of the azomethine group, which is essential for biological activity and coordinated behavior [3] .Schiff bases' biochemical significance, electrochemical characteristics, and a range of pharmacological functions, including antifungal, antiviral, antimalarial, anti-inflammatory, and catalytic activity, have all been well studied over the years. [1,2]. In addition to these applications, they have been successfully utilized in industrial processes as corrosion inhibitors, thermally stable materials, and efficient ligands for the synthesis of coordination compounds[3].

Schiff bases derived from various amines have been synthesized and structurally characterized in a number of investigations, several of which showed significant antibacterial action against both Gram-positive and Gram-negative microbes [4]. Schiff base ligands continue to get a lot of interest in metal coordination chemistry despite being discovered almost a century ago because of their high metal-binding ability, simplicity of synthesis, and structural flexibility[5]. These features make them valuable building

*Author for Correspondence: korejb5145@gmail.com

blocks for the development of metallo-organic materials and functional coordination compounds[6,7].

Due to its potential uses in fields including materials science, molecular magnetism, and catalysis, macrocyclic Schiff base complexes have attracted increasing attention in recent years[6,7]. Schiff base complexes have been shown to participate effectively in various chemical transformations, including oxidation, reduction, and carbonization reactions, as well as in metal ion binding and transport processes[8]. Furthermore, these compounds have found industrial applications as pigments, polymer stabilizers, and catalysts in polymerization and redox reactions[9]. From a biomedical perspective, Numerous biological actions, including as antibacterial, antifungal, antiviral, antimalarial, antiproliferative, and antipyretic properties, are known to be exhibited by schiff bases[10-13] .

The current work focuses on the synthesis, spectroscopic characterization, and thermal analysis of a novel Mannich–Schiff base ligand, 1–[(2–{1–[(dicyclohexylamino)–methyl]–1H–indol–3–yl}ethylimino)methyl]–naphthalen–2–ol (HL), along with its metal complexes, as part of continuing research on Schiff base chemistry[14]. The experimental investigations are further supported by density functional theory (DFT) calculations to provide deeper insight into the structural and electronic properties of the synthesized compounds.

1. EXPERIMENTAL:

1.1 Materials and methods-

All chemicals and solvents were of analytical grade and obtained from commercial sources. Calcium chloride ($CaCl_2$), chromium(III) chloride hexahydrate ($CrCl_3 \cdot 6H_2O$), manganese(II) chloride tetrahydrate ($MnCl_2 \cdot 4H_2O$), iron(III) chloride dihydrate ($FeCl_3 \cdot 2H_2O$), palladium(II) chloride ($PdCl_2$), cadmium chloride dihydrate ($CdCl_2 \cdot 2H_2O$), mercuric chloride ($HgCl_2$), 2-hydroxy-1-naphthaldehyde, dicyclohexylamine, and 2-(1H-indol-3-yl)ethylamine were used without additional purification. Methanol, ethanol, and dimethyl sulfoxide (DMSO) were supplied by Merck.

1.2 Physical measurements-

All chemicals employed in the present investigation were obtained from commercial suppliers and utilized without further purification. Solvents were freshly distilled over suitable drying agents prior to use. Elemental (C, H, and N) analyses were carried out using a PerkinElmer 2400 CHN elemental analyzer. The metal content of the synthesized complexes was determined gravimetrically by converting the metals into their corresponding oxides. Molar conductance measurements of the ligand and its metal complexes were performed in DMSO at a concentration of 1×10^{-3} mol L^{-1} using a Jenway 4010 conductivity meter. Magnetic susceptibility measurements were recorded at room temperature using a

Sherwood Scientific magnetic balance following the Gouy method. Electron impact mass spectra (70 eV) were obtained on a Finnigan-MAT 8430 GC–MS-DS instrument. A Jenway 6405 UV–Vis spectrophotometer with 1 cm quartz cells was used to record the electronic absorption spectra of the ligand and its metal complexes in DMF solution (1×10^{-3} M) spanning the wavelength range of 200–900 nm. KBr pellets were used to measure infrared spectra in the 4000–400 cm^{-1} range using a Bruker FT-IR spectrophotometer. Using a Bruker AMX 400 MHz spectrometer and tetramethylsilane (TMS) as the internal reference, H1 NMR spectra were obtained in DMSO-d^2. Using a Perkin Elmer Pyris Diamond DTA/TG thermal analyzer in a nitrogen environment, the thermal behavior of the ligand and its metal complexes was examined over a temperature range of 25–700 °C at a heating rate of 10 °C min^{-1}.

1.3 Synthesis of Schiff base (HL)-

Schiff bases are typically synthesized through the condensation reaction between primary amines and carbonyl compounds. This process involves an initial nucleophilic addition leading to the formation of a hemiaminal intermediate, which subsequently undergoes dehydration to yield the corresponding imine derivatives (Scheme 1). Since the first report of Schiff base formation in the nineteenth century[15], numerous synthetic strategies have been developed and documented in the literature. The commonly employed methods are outlined below:

1.3.1 Preparation of 1-{[2-(1H-Indol-3-yl) ethylimino] methyl}-naphthalen-2-ol (A)

A condensation reaction involving 2-hydroxy-naphthalene-1-carbaldehyde (0.01 mmol) and 2-(1H-indol-3-yl)ethylamine (0.01 mmol) in ethanol as the reaction medium produced the title chemical. Thin-layer chromatography (TLC) was used to track the reaction's progress while the resultant mixture was agitated and refluxed at 85 °C for three hours. A solid product was formed when the reaction mass was allowed to cool to room temperature after it was finished. Filtration was used to gather the precipitate, which was then carefully cleaned with cold ethanol. recrystallized from hot ethanol to improve purity, and finally dried under reduced pressure.

1.3.2 Preparation of 1-[(2-{1-[(dicyclohexylamino)-methyl] 1H-indol-3-yl}-ethylimino)-methyl]-naphthalen-2-ol (HL)

Aqueous formaldehyde solution (37% v/v) was added dropwise after the Schiff base (10 mmol) and dicyclohexylamine (10 mmol) reacted. To regulate the reaction temperature, the reaction mixture was constantly agitated for about three hours while being periodically cooled. The resulting solution was then stored in a refrigerator for 12 h, during which a fine precipitate gradually formed. Excess petroleum ether was subsequently added to the suspension, and crystallization was induced by gently scratching the inner surface of the vessel with a glass rod, leading to rapid solidification of the product. Filtration was used to gather the precipitate, which was then carefully cleaned with 15 mL of

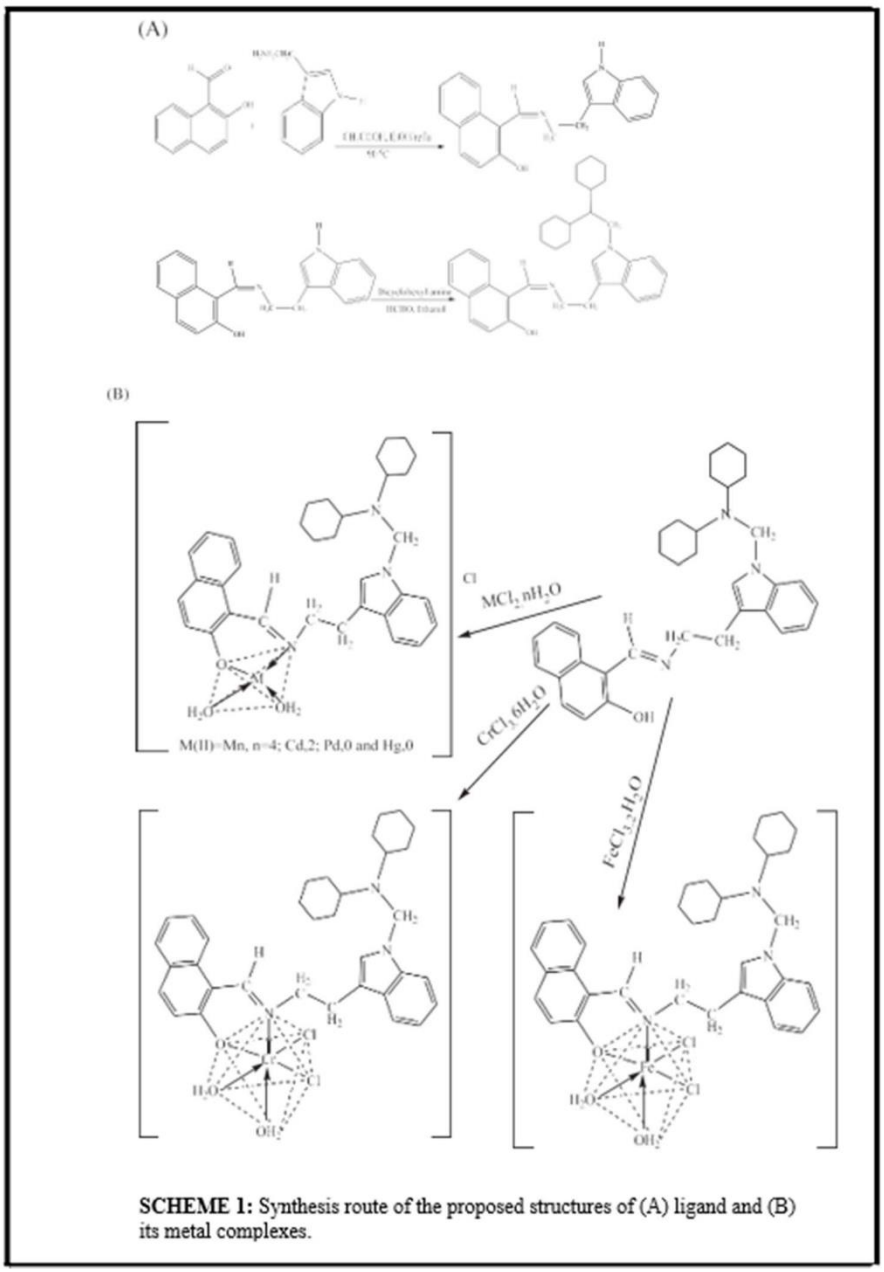

SCHEME 1: Synthesis route of the proposed structures of (A) ligand and (B) its metal complexes.

SCHEME 1: Synthesis route of the proposed structures of (A) ligand and (B) its metal complexes.

petroleum ether and allowed to dry at room temperature. Recrystallization from ethanol was used to further purify the crude product. Table 1 summarizes the molecular formula, molecular weight, melting point, percentage yield, and elemental analytical data. ^{1}H NMR (DMSO-d_6, δ ppm): 9.08 (s, 1H, –CH═N),
7.18–7.99 (m, 10H, aromatic), 5.99 (s, 1H, –OH), 4.49 (s, 2H, –CH_2–), 3.10 (m,
20H, cyclohexyl –CH_2–), 2.69 (t, 4H, –CH_2–); solvent signal at δ 2.50 (DMSO).

1.4 Synthesis of Schiff base Metal complexes-

The corresponding hydrated metal salts, $VOSO_4 \cdot H_2O$, $CrCl_3 \cdot 6H_2O$, $MnCl_2 \cdot 4H_2O$, $FeCl_3 \cdot 2H_2O$, and $PdCl_2$ (1 mmol), were gradually added to a stirred ethanolic solution (20 mL) of the ligand L1 (0.295 g, 1 mmol) to create the metal complexes of the Schiff base ligand (L1). For one to one and a half hours, the reaction mixture was continuously stirred at room temperature. The resultant colorful precipitates were purified by recrystallization from a methanol–chloroform combination (1:3, v/v), separated by filtering, and extensively cleaned with 100% ethanol to eliminate unreacted species. The isolated complexes were dried under reduced pressure over anhydrous calcium chloride. The physical characteristics, elemental analysis

results, colors, and percentage yields of the synthesized complexes are summarized in (Table 1).

TABLE 1: Analytical and physical data of the ligand and its complexes.

Compounds	Formula m. wt	Color	m. p °C	Yield %	Elemental analysis, found / Calc.%				
					C	H	N	M	Cl
HL	C34H41N3O 507.71	Orange	188-190	88	81.21	7.99	7.97		
					80.43	8.14	8.28		
[Mn (L) (H2O)2]Cl	C34H44N3O3ClMn 633.12	Light yellow	232d	69	63.66	7.62	7.18	10.01	6.27
					64.50	7.00	6.64	8.68	5.60
[Pd (L) (H2O)2]Cl	C34H44N3O3ClPd 684.60	Red-brown	210d	60	60.74	5.78	7.97	14.07	5.79
					59.65	6.48	6.14	15.54	5.18
[Cd (L) (H2O)2]Cl	C34H44N3O3ClCd 690.60	Light brown	194d	81	60.86	7.29	7.55	17.31	5.87
					59.13	6.42	6.08	16.28	5.13
[Hg (L) (H2O)2]Cl	C34H44N3O3ClHg 778.77	Light brown	182d	77	54.33	5.93	7.04	23.98	5.51
					52.44	5.69	5.40	25.76	4.55
[Cr(L)(H2O)2Cl2]	C34H44N3O3Cl2Cr 665.63	Dark green	215d	82	62.78	5.31	7.49	8.76	13.05
					61.35	6.66	6.31	7.81	10.65
[Fe(L)(H2O)2Cl2]	C34H44N3O3Cl2Fe 669.48	Red-brown	217d	73	61.14	5.77	7.45	10.05	9.97
					61.00	6.62	6.28	8.34	10.59

1.5 Microbiological investigations-

The antimicrobial activity of the synthesized Schiff base ligand, its metal complexes, and the corresponding metal salts was evaluated against Staphylococcus aureus (Gram-positive) and Pseudomonas aeruginosa (Gram-negative) bacterial strains, as well as fungal species including Penicillium expansum, Fusarium graminearum, Macrophomina phaseolina, and Candida albicans. The screening was carried out using the agar well diffusion method with dimethyl sulfoxide (DMSO) as the solvent. Test solutions were prepared at a concentration of 1×10^{-3} M and applied using the disc diffusion technique. Antimicrobial efficacy was assessed by measuring the diameter of the inhibition zones formed due to the diffusion of the test compound into the agar medium. The inoculated plates were incubated at 37 °C for 24 h for bacterial strains and 48 h for fungal strains.

1.6 Programs used in theoretical calculation-

HyperChem 8 is an advanced molecular modeling and computational chemistry software that integrates molecular visualization and animation with quantum chemical calculations, molecular mechanics, and molecular dynamics simulations. The program is widely recognized for its reliability, versatility, and user-friendly interface. In the present study, the semiempirical parameterization method 3 (PM3) was employed to compute the heats of formation and binding energies of the synthesized metal complexes. PM3, along with the AMBER force field, is among the most frequently used semiempirical approaches due to the availability of robust computational algorithms and its improved accuracy compared to other related methods [14]. The PM3 method has been primarily parameterized for organic systems and selected transition metal ions[16,17].

1.7 The thermal analysis-

Analysis of the thermogravimetric (TGA) curves recorded for the Schiff base ligand and its metal complexes enabled the determination of key thermal parameters corresponding to each stage of the decomposition process. The initial decomposition temperature (T_i) was defined as the temperature at which the TG curve begins to depart from the baseline, while the final decomposition temperature (Tf) corresponds to the point at which the curve stabilizes and returns to the baseline. The peak decomposition temperature (TDTG), representing the temperature of maximum rate of mass loss, was obtained from the maximum of the differential thermogravimetric (DTG) curve. The mass loss associated with each decomposition step (Δm) was calculated from the difference in sample mass between T_i and Tf, as indicated by the ordinate of the TG curve. The nature of the fragments released during each stage was assigned by comparing the experimental mass loss values with those theoretically calculated from the molecular formulas of the investigated complexes. These assignments were further supported by comparison with reported thermal behavior of structurally related compounds and by considering the corresponding decomposition temperature ranges. The activation energy (E_a) for the decomposition steps was evaluated using the integral method based on the Coats–Redfern equation[18]. For reaction orders $n \neq 1$ or $n = 1$, appropriate linearized plots were obtained by selecting the correct kinetic model, and the activation energy values were calculated from the slopes of the resulting straight-line plots.

$$Log\left[\frac{1-(1-\alpha)^{1-n}}{T^2(1-n)}\right] = Log\left[\left(1-\frac{2RT}{E_a}\right)\right] - \frac{E_a}{2.303RT} \quad for \neq 1$$

$$Log\left[\frac{-\log(1-\alpha)}{T^2}\right] = Log\left[\frac{ZR}{qE_a}\left(1-\frac{2RE}{E_a}\right)\right] \frac{E_a}{2.303RT} for = 1$$

The thermodynamic parameters associated with the decomposition process were evaluated using the following relationships: the entropy of activation (ΔS*) was calculated using the expression,

ΔS* = 2.303 R [log (Ah / kT_max)],

while the enthalpy of activation (ΔH*) was obtained from, **ΔH* = E − RT_max**.

The Gibbs free energy of activation (ΔG*) was determined using the relation **ΔG* = ΔH* − T_maxΔS***.

In these expressions, α represents the fraction of mass loss, T is the absolute temperature (K), n denotes the reaction order, A (or Z) is the pre-exponential factor, R is the universal gas constant, E is the activation energy, and q corresponds to the heating rate. The reaction order (n) was selected as the value that produced the best linear fit of the Coats–Redfern plots among several trial values and was further validated by comparison with values estimated using the Horowitz–Metzger method.

RESULTS AND DISCUSSION:

The Schiff base ligand was synthesized in good yield by refluxing 1-{[2-(1H-indol-3-yl)-ethylimino]methyl}naphthalen-2-ol with dicyclohexylamine in ethanol (Scheme 1). The ligand was characterized by EA (Table 1), IR (Table 2), UV-vis (Table 3), and mass spectroscopy. Complexation of the ligand with $VOSO_4 \cdot H_2O$, $CrCl_3 \cdot 6H_2O$, $MnCl_2 \cdot 4H_2O$, $FeCl_3 \cdot 2H_2O$, and $PdCl_2$ afforded monomeric metal complexes of the type $[M(II)(L)(H_2O)_2]Cl$ (M = Mn, Pd, Cd, Hg) and $[M(III)(L)(H_2O)_2Cl_2]$ (M = Cr, Fe). The complexes are air-stable solids, soluble in DMF and DMSO, and their elemental analysis data agree well with the proposed structures[19,20].

Infrared spectra-

The FT-IR spectrum of the free Schiff base ligand (HL) showed characteristic bands at 3462, 3035, 2960, 2905, and 1673 cm^{-1}, corresponding to ν(OH) phenolic, ν(C–H) aromatic, ν(C–H) aliphatic, ν(C–H) aldehydic, and ν(C═N) azomethine vibrations, respectively[21]. Upon complexation, these bands exhibited noticeable shifts, confirming coordination[22]. The ν(C═N) stretching frequency of the ligand (1660–1644 cm^{-1}) shifted to lower wavenumbers by 13–29 cm^{-1} in the metal complexes, indicating involvement of the azomethine nitrogen in coordination. Additional bands observed in the regions 523–459 cm^{-1} and 467–411 cm^{-1} were assigned to ν(M–N) and ν(M–O) vibrations, respectively. The appearance of new

bands around 3562–3547 cm^{-1} and 874–828 cm^{-1}, attributed to $\nu(H_2O)$ and $\delta(H_2O)$ modes, confirmed the presence of coordinated water molecules. These observations suggest that the ligand coordinates to the metal ions through the phenolic oxygen and azomethine nitrogen atoms[23,24].

Mass spectrum-

1.7.1 Synthesis of Ligand-

The electron impact mass spectrum of the Schiff base ligand (HL) exhibited a molecular ion peak at *m/z* 507, which corresponds to the calculated molecular mass of the ligand ($C_{34}H_{41}N_3O$, 507.71), thereby confirming its proposed structure. Additional fragment ion peaks observed at *m/z* 491, 353, and 142 arise from characteristic fragmentation of the Schiff base framework. The relative intensities of these peaks reflect the stability of the corresponding fragment ions.

1.7.2 Synthesis of Cr(III) complex-

The electron impact mass spectrum of the chromium(III) complex $[Cr(L)(H_2O)_2Cl_2]$ displayed a molecular ion peak at *m/z* 665, which is consistent with the calculated molecular mass of the complex ($C_{34}H_{44}N_3O_3Cl_2Cr$, 665.63), thereby supporting the proposed composition. Fragment ion peaks observed at *m/z* 629 and 365 arise from stepwise fragmentation of the complex framework.

1.7.3 Synthesis of Cu (II) complex-

The electron impact mass spectrum of the iron(III) complex $[Fe(L)(H_2O)_2Cl_2]$ exhibited a molecular ion peak at *m/z* 669, which agrees well with the calculated molecular mass of the complex ($C_{34}H_{44}N_3O_3Cl_2Fe$, 669.48), confirming the proposed formulation. Additional fragment ion peaks observed at *m/z* 633, 562.5, 337.5, and 225 are attributed to successive fragmentation of the complex.

1.7.4 Synthesis of Mn(II) complex-

The electron impact mass spectrum of the manganese(II) complex $[Mn(L)(H_2O)_2]Cl$ exhibited a molecular ion peak at *m/z* 597.5, which is in good agreement with the calculated molecular mass of the complex ($C_{34}H_{44}N_3O_3Mn$, 597.67), thereby confirming the proposed structure. Fragment ion peaks observed at *m/z* 561, 367, 196, and 171 arise from characteristic fragmentation of the complex framework.

1.8 Electronic absorption spectra, magnetic moments, and conductivity measurements-

The electronic spectrum of the free Schiff base ligand (HL) displayed intense absorption bands at 282 and 330 nm, assigned to π→π* transitions, along with a band at 348 nm corresponding to n→π* transitions. The Cr(III) complex exhibited three absorption bands at 535, 645, and 905 nm, which were attributed to the ^4A_2g → $^4T_1g(P)$, ^4A_2g → $^4T_1g(F)$, and ^4A_2g → $^4T_2g(F)$ transitions, respectively, consistent with an octahedral environment. The Fe(III) complex showed an absorption band at 462 nm, assignable to the ^5T_2g → ^5E_g transition. The magnetic moment values of the Cr(III) (d^3) and Fe(III) (d^5) complexes were found to be 3.05 and 5.01 B.M., respectively. These μeff values are in agreement with high-spin octahedral geometries around the central metal ions.

The electronic spectrum of the Pd(II) complex exhibited two broad bands at 493 and 765 nm, which were assigned to the ^1A_1g → ^1B_1g and ^1A_1g → ^1A2g transitions, respectively, indicating a square-planar geometry. The Mn(II) complex showed two broad absorption bands at 418 and 568 nm, attributable to the $^6A_1$ → $^4T_2(G)$ and

TABLE 2: FTIR spectral data (wavenumber ύ) cm−1 for the ligand and its complexes.

Compounds	υ(OH)	υ(CH) aromatic	υ(CH) aliphatic	υ(CH) aldehyde	υ(C = N)	υ(M-N)	υ(M-O)	H2O rocking
HL	3462	3035	2960	2905	1673	-	-	
[Mn (L) (H2O)2]Cl	-	3044	2958	2909	1660	511	445	3547 874
[Pd (L) (H2O)2]Cl	-	3051	2945	2941	1649	523	433	3562 870
[Cd (L) (H2O)2]Cl	-	3077	2965	2919	1658	509	467	3557 828
[Hg (L) (H2O)2]Cl	-	3033	2977	2923	1651	487	440	3549 829
[Cr(L)(H2O)2Cl2]	-	3046	2951	2916	1644	521	436	3555 848
[Fe(L)(H2O)2Cl2]	-	3044	2974	2898	1659	459	411	3569 837

TABLE 3: Electronic data and molar conductivity for the metal complexes.

								Suggested

Complexes	λ Nm	Assignment	Ω ohm−1 cm 2 mol−1	μeff B.M.	formula
[Mn (L)(H2O)2]Cl	418	^{6}A1 → ^{4} T2(G)	78	5.11	Tetrahedral
	568	^{6}A1 → ^{4} T1(G)			
[Pd (L) (H2O)2]Cl	493	^{1}A1g → ^{1}B1g ^{1}A1g → ^{1}A2g	76	Diamagnetic	Square planer
	765				
[Cd (L) (H2O)2]Cl	395	C.T	88	Diamagnetic	Tetrahedral
[Hg (L) (H2O)2]Cl	385	C. T	86	Diamagnetic	Tetrahedral
[Cr(L)(H2O)2Cl2]	535	^{4}A2g → ^{3}T1g p, ^{4}A2g → ^{3}T1g	21	5.01	Octahedral
	645	pF ^{4}A2g → ^{3}T2g F			
	905				
[Fe(L)(H2O)2Cl2]	409	C. T	15	3.05	Octahedral
	462	^{5}T2g → ^{5}Eg			

$^6A_1$ → $^4T_1$(G) transitions, respectively[32,33]. Only charge-transfer bands were visible in the Cd(II) and Hg(II) complexes at 385 and 395 nm, respectively, consistent with their d^{10} electronic configurations and diamagnetic

nature, confirming the absence of d–d transitions. The magnetic moment of the Mn(II) (d^5) complex was found to be 5.11 B.M., while the Cd(II) and Hg(II) complexes were diamagnetic. These spectral and magnetic data support a tetrahedral geometry for these complexes[25]. The molar conductance values indicated 1:1 electrolytic behavior for most complexes, whereas the Cr(III) and Fe(III) complexes behaved as non-electrolytes. All electronic transitions are summarized in (Table 3), and the proposed structures of the metal complexes are illustrated in (Scheme 1).[32,26]

1.9 Study complexes in gas stat (theoreticalstudies)-

1.9.1 Electrostatic potentials-

The electron distribution within a molecule governs its electrostatic potential (EP), which represents the interaction energy between the molecular system and a positive test charge. Analysis of EP is useful for identifying reactive regions in a molecule, as electrophilic species preferentially attack sites with negative electrostatic potential [27]. In the present study, the electrostatic potential of the free Schiff base ligand (HL) was calculated and represented as a two-dimensional contour map (Figure 1) to locate its probable reactive sites. In addition, the reactivity and stereochemical behavior of the ligand were interpreted in terms of frontier molecular orbitals, namely the highest occupied molecular orbital (HOMO) and the lowest unoccupied molecular orbital (LUMO). The computational results indicate that coordination occurs through the HOMO localized mainly on the azomethine nitrogen and phenolic oxygen atoms of the ligand, which preferentially interact with the LUMO of the metal ions during complex formation.

1.9.2 Optimized energies-

Semiempirical and molecular mechanics calculations were performed using the Hyper Chem-8 program. The heats of formation (ΔH°_f) and binding energies (ΔE_b) of the free ligand and its metal complexes were calculated, and the results are summarized in (Table 4).

1.9.3 Optimized vibrational spectra for ligand (HL)-

The vibrational spectra of the free ligand and its metal complexes were calculated using computational methods, and the results are presented in (Table 5). While some deviations between the calculated and experimental wavenumbers are expected, the theoretically predicted frequencies showed good agreement with the experimental values (Table 2) [28] . The most diagnostic vibrational modes were selected for assigning the key functional groups of the ligand (HL) and its complexes, as summarized in (Tables 2 & 5).

1.9.4 Bond length measurements for the (HL) and their metal complexes-

The geometrical parameters, including optimized bond lengths, of the free ligand (HL) and its metal complexes were determined using the semi-empirical PM3 method at a geometry optimization criterion of 0.001 K.Cal·mol^{-1}. The results showed excellent agreement with the experimental values, as presented in (Table 6)[29,30].

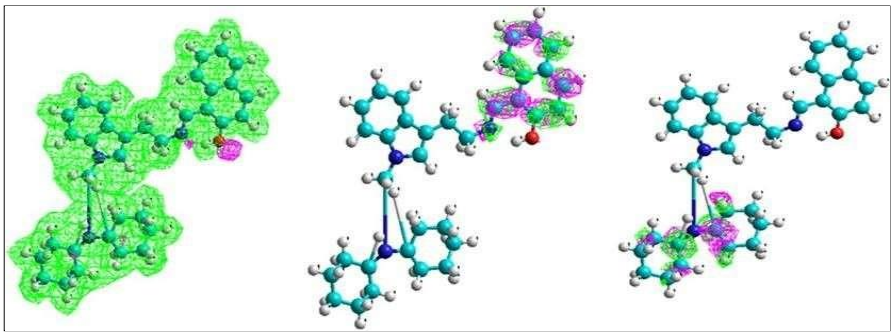

FIGURE 1: Electrostatic potential (HOMO & LUMO) as 2D contours for (HL)

1.9.5 Theoretical electronic spectra for the metal complexes-

As shown in Table 7, the estimated wavenumbers of the metal complexes' electronic spectra showed some variations from the experimental values. Because they result from couplings between electronic spectral modes and the presumption that each normal mode interacts independently with the electronic spectral beam, such differences in theoretical computations are typically regarded as acceptable[31].

TABLE 4: Conformation energetic (in KJ.mol−1) for Naringin and its metal complexes.

Compounds	ΔE tot	ΔH^{o}_{f}	ΔE*b*	Dipole (Debyes)
HL	−125392.57133	102.2404773	−8242.7605227	4.581
[Mn (L) (H2O)2]Cl	−122628.72311	2115.401668	−986.4163316	4.648
[Cr(L)(H2O)2Cl2]	−135141.76535	1781.34446	−4482.78009	3.106
[Cd (L) (H2O)2]Cl	−194751.1675	1742.1165	−5998.176532	5.112
[Fe(L)(H2O)2Cl2]	−20848.11537	1553.5667	−6859.1997001	5.142
[Pd (L) (H2O)2]Cl	−1096.463316 (Amber)			8.120
[Hg (L) (H2O)2]Cl	−3757.82801 (Amber)			4.451

TABLE 5: Comparison between the experimental and theoretical vibrational frequencies (cm^{-1}) for free ligand (HL) metal complexes.

Compounds	υ C = N		υ M-N		υ M-O		H2O rocking	
HL	1677[a]	1673[b]	-		-		-	
[Mn (L) (H2O)2]Cl	1653[a]	1660[b]	505[a]	511[b]	491[a]	445[b]	882[a]	874[b]
[Pd (L) (H2O)2]Cl	1655[a]	1649[b]	563[a]	523[b]	465[a]	433[b]	850[a]	870[b]
[Cd (L) (H2O)2]Cl	1640[a]	1658[b]	546[a]	509[b]	501[a]	467[b]	836[a]	828[b]
[Hg (L) (H2O)2]Cl	1645[a]	1651[b]	435[a]	487[b]	495[a]	440[b]	835[a]	829[b]
[Cr(L)(H2O)2Cl2]	1640[a]	1644[b]	581[a]	521[b]	488[a]	436[b]	855[a]	848[b]
[Fe(L)(H2O)2Cl2]	1644[a]	1659[b]	477[a]	459[b]	488[a]	411[b]	853[a]	837[b]

Where,

[a]Theoretical frequency, [b]Experimental frequency.

TABLE 6: Selected bond lengths (A°) for (E) ligand and their metal complexes.

Compounds	C = N	C-O	M-N	M-O	M-Cl
HL	1.347	1.363	-	-	-
[Mn (L) (H_2O)$_2$]Cl	1.450	1.354	1.689	1.944	1.889
[Pd (L) (H2O)2]Cl	1.449	1.360	1.690	1.946	1.978
[Cd (L) (H_2O)$_2$]Cl	1.441	1.355	1.689	1.944	1.899
[Hg (L) (H2O)2]Cl	1.441	1.355	1.691	1.945	1.898
[Cr(L)(H2O)2Cl2]	1.352	1.351	1.690	1.946	1.954
[Fe(L)(H2O)2Cl2]	1.351	1.358	1.689	1.946	1.954

For the purpose of assigning the metal complexes, the most diagnostically important computed electronic spectra were chosen. Table 3 lists the experimental electronic transitions. After geometry adjustment, the theoretical electronic spectra of the compounds under study were produced using the semi-empirical PM3 method at an energy convergence of 0.01 K.Cal·mol^{-1}. Table 7 shows a comparison of the estimated and observed electronic spectrum data for the metal complexes[34,35].

1.9.6 Optimized geometries of HL and their complexes-

All theoretically possible structures of the free ligand and its metal complexes were optimized using the PM3 method in the gas phase to identify the most probable and energetically stable structural models, as illustrated in Figure 2.

TABLE 7: Comparison between experimental and theoretical of the electronic spectra for complexes.

Complexes	Maximum	absorption (nm)	Band assignment	Suggested geometry
[Mn (L) (H2O)2]Cl	577[a] 624[a]	 418[b]	$^6A1 \rightarrow {}^4T2(G)$ $^6A1 \rightarrow {}^4T1(G)$	Tetrahedral
		568[b]		
[Pd (L) (H2O)2]Cl	557[a] 687[a]	493[b] 765[b]	$^1A1g \rightarrow {}^1B1g$ $^1A1g \rightarrow {}^1A2g$	Tetrahedral
[Cd (L) (H2O)2]Cl	453[a]	395[b]	C.T	Tetrahedral
[Hg (L) (H2O)2]Cl	485[a]	385[b]	C. T	Tetrahedral
[Cr(L)(H2O)2Cl 2]	457[a] 687[a]	535[b] 645[b]	$^4A2g \rightarrow {}^3T1g$ p, $^4A2g \rightarrow {}^3T1g$ pF $^4A2g \rightarrow {}^3T2g$ F	Octahedral
	876[a]	905[b]		
[Fe(L)(H2O)2Cl2]	492[a] 590[a]	409[b] 462[b]	C. T $^5T2g \rightarrow {}^5Eg$	Octahedral
[a]Theoretical frequency.				
[b]Experimental frequency				

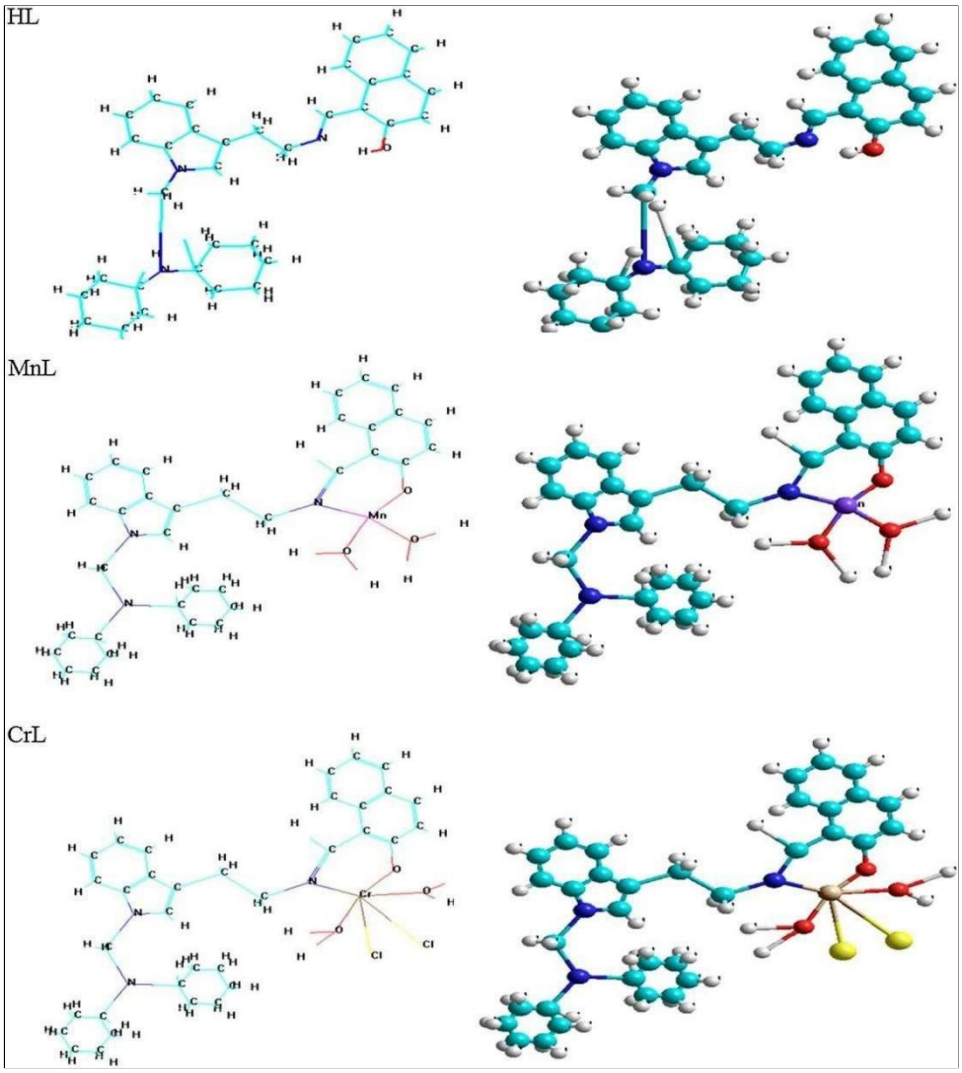

FIGURE 2: Conformational structure of (HL) and their metal complexes.

1.10 Thermal analysis-

To assess the Schiff base ligand's and its metal complexes' thermal stability, thermal analysis was performed. Under a nitrogen environment, thermogravimetric measurements were conducted between 25 and 700 °C at a heating rate of 10 °C min^{-1}. The estimated values and the experimental mass losses agreed quite well, confirming the proposed molecular compositions and elemental analysis results (Table 8).

(HL)-C34H41N3O [99.34%Found (100%Cal)]
199.1-313.7°C →C12 H16N [29.8%Found (29.53%Cal)]
313.7-589.3°C →C22H25N2O [69.54%Found (70.47%Cal)] (CrL)-C34H44N3O3CrCl2 [89.011%Found (89.542%Cal)]
33.5-139.8°C → 2H2O [4.163%Found (5.408%Cal)]
139.8-389.7°C → 2Cl + C13H23N [40.794%Found (39.515%Cal)]

389.7-698.4°C →C21H17N2 [44.054%Found (44.619%Cal)]

(MnL)-C34H44N3O3MnCl [84.644%Found (83.08%Cal)]
35.5-118.9°C → 2H O [4.981%Found (5.686%Cal)]
118.9-304°C → C15H10Cl [29.612%Found (30.168%Cal)]
304-689.5°C → C10H30N3 [50.051%Found (47.226%Cal)]

The Schiff base showed a first step of breakdown that corresponded to the loss of a C12H16N3 fragment, and then the remaining ligand framework gradually degraded. The appropriate metal oxides were formed as a result of the metal complexes' last step of breakdown (Table 9).

TABLE 8: Thermal analysis data of some metal complexes of HL.

% estimated (calculated)					
Com.	**TG range (°C)**	**DTG max (°C)**	**Mass loss**	**Total mass loss**	**Assignment**
HL	199.1-313.7	287.9	29.8(29.53)	99.34	C12H16N
		524.4	69.54(70.47)	(100)	C22H25N2O
	313.7-589.3				
CrL	33.5-139.8	71.12	4.163(5.408)	89.011	2H2O
	139.8-389.7	288	40.794(39.515)	(89.542)	C13H23 NCl2
		504			
	389.7-698.4		44.054(44.619)		C21H17N2 CrO+
MnL	35.5- 118.9	89.5	4.981 (5.686)	84.644	2H2O
	118.9- 304	235	29.612 (30.168)	(83.08)	C15H19 N2 Cl
	304- 689.5	482	50.051 (47.226)		C22H21N
					MnO

TABLE 9: Thermodynamic data of the thermal decomposition of ligand and their complexes

Sam	**T range (°C)**	**n**	**R2**	**Tmax (K)**	**Ea (kJ mol−1)**	**ΔH* (kJ mol−1)**	**A (s−1 × 10^7)**	**ΔS* (J mol−1 K−1)**	**ΔG* (kJ mol−1)**	**K × 10−7**
HL	199.1-313.7	1	0.997	287.9	10.160737	5.707551	3.661	−104.996	61.946	9.09510
HL	313.7-589.3.	1	0.998	524.4	13.851965	13.1808	7.791	−102.075	95.086	6.45457
CrL	33.5-139.8	0.9	0.995	71.12	6.16778	3.79795	2.4383	−89.589	41.4703	6.2516
CrL	139.8-389.7	0.9	0.991	288	10.4435	4.1547	5.4487	−88.137	68.8081	0.19629
CrL	389.7-698.4	0.9	0.991	504	14.463755	8.4279	6.5654	−87.93	85.4412	0.44099
MnL	35.5-118.9	0.9	0.998	89.5	8.209644	3.357	2.82715	−118.68	49.8031	0.11652
MnL	118.9-304	0.9	0.989	235	13.4215	5.4185	13.0333	−108.2493	77.8435	0.23090
MnL	304-689.5	0.9	0.997	482	17.1548	7.957	15.97571	−79.445	107.4027	0.55368

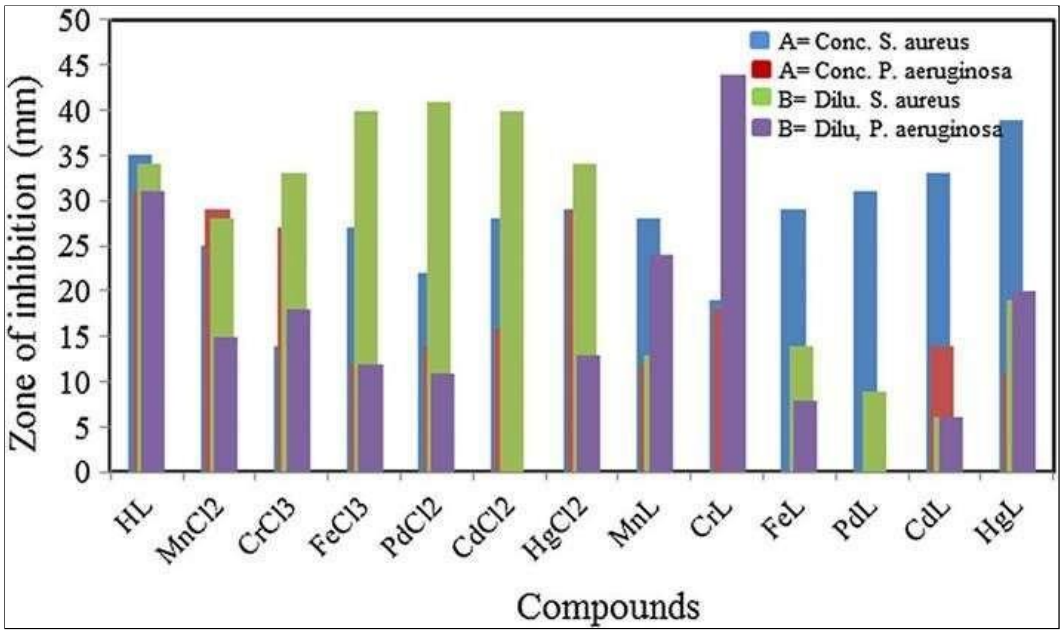

FIGURE 3: The antibacterial activity of compounds against S. aureus and P. aeruginosa.

1.11 Antimicrobial activity of ligand and all complexes-

The bacterial strains Staphylococcus aureus and Pseudomonas aeruginosa, as well as the fungal strains Penicillium expansum, Fusarium graminearum, Macrophomina phaseolina, and Candida albicans, were used to test the biological activity of the Schiff base ligand and its metal complexes. Figures 3–6 describe the findings, which were contrasted with the DMSO standard control. In contrast to its metal complexes and equivalent metal salts, the free ligand demonstrated moderate antibacterial activity against S. aureus and P. aeruginosa. The ligand alone displayed negligible antifungal activity; however, several metal complexes and metal salts demonstrated significant antifungal effects.

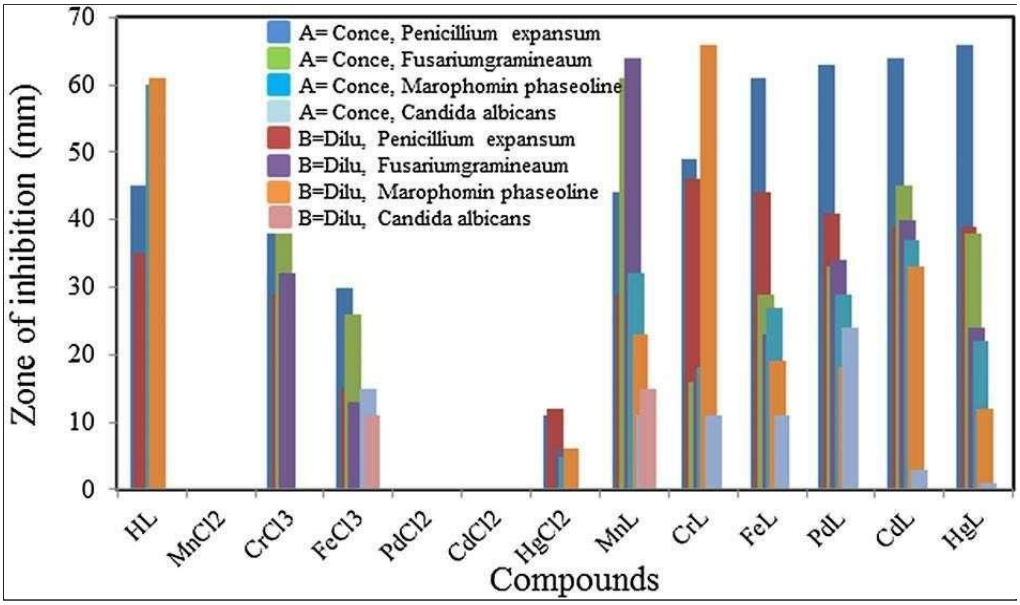

FIGURE 4: The antibacterial activity of compounds against P expansum and F graminearum.

In particular, CrL and FeL complexes showed lower activity than their respective metal salts against P. expansum and F. graminearum. Overall, the results indicate that coordination with metal ions enhances the antimicrobial efficacy of the Schiff base, likely due to the influence of the central metal ion (Figures 4–6).

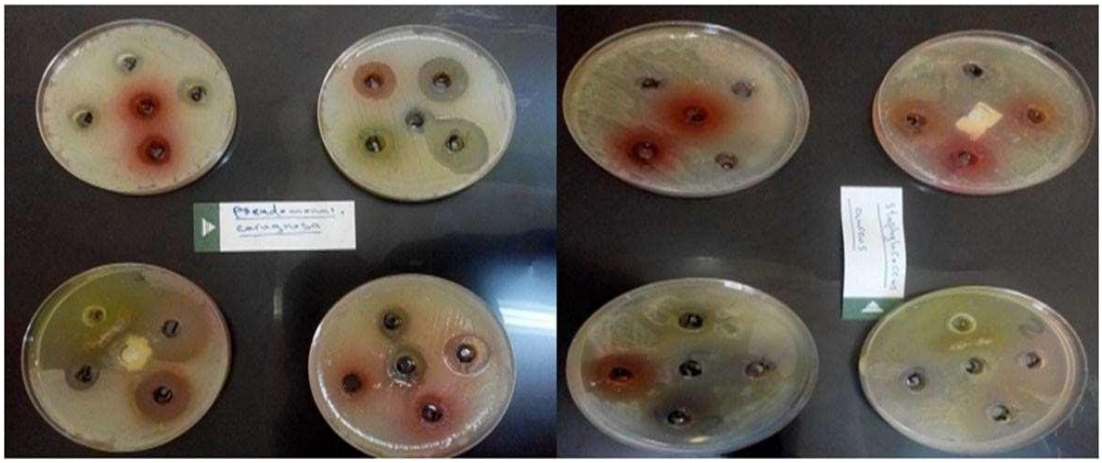

FIGURE 5: Effect of the ligand complexes towards the Staphylococcus aureus and Pseudomonas aeruginosa.

FIGURE 6: Effect of the ligand and complexes towards the Penicillium expansum.

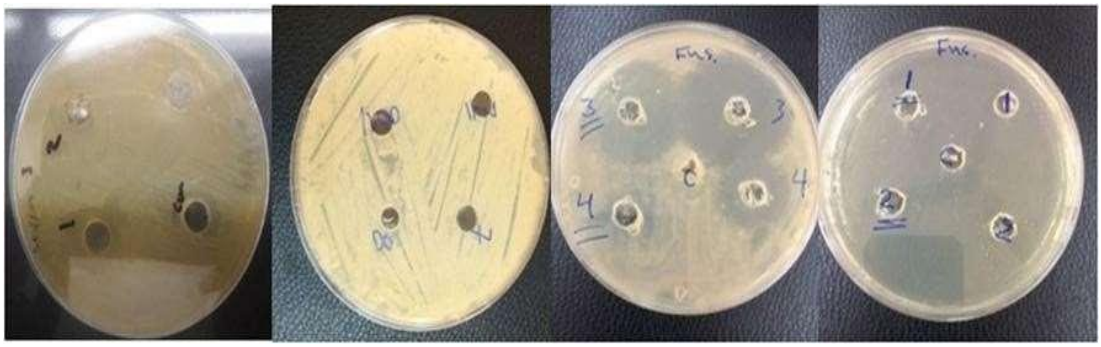

FIGURE 7: Effect of the ligand and complexes towards the Fusarium graminearum.

FIGURE 8: Effect of the ligand and complexes towards the Macrophomina phaseolina.

FIGURE 9: Effect of the ligand and complexes towards the Candida albican.

CONCLUSION:

The current study effectively synthesized and thoroughly characterized a Schiff base ligand and its associated metal complexes. The suggested compositions and coordination modes of the synthesized compounds were validated by elemental analysis, spectroscopic methods (FT-IR, ^{1}H NMR, and mass spectrometry), thermal analysis, magnetic moment measurements, and molar conductance tests. The creation of stable metal–ligand assemblies was further confirmed by the complexes' non-electrolytic nature and their reported magnetic behavior. The experimentally derived structural features showed good correlation with theoretical molecular orbital calculations, confirming the ligand's and its metal complexes' optimal geometries and bonding properties. The kinetic and thermodynamic parameters (ΔE^*, ΔH^*, ΔS^*, ΔG^*, and K), which were determined from TGA data using the Coats–Redfern method, showed that the complexes have significant thermal stability and adhere to clearly defined decomposition mechanisms. Thermal decomposition studies also revealed multi-step degradation patterns. A biological analysis showed that the Schiff base's antibacterial activity was greatly increased by metal coordination. Several metal complexes showed better inhibitory effects against the studied bacterial strains than the free ligand, according to the agar diffusion method. While DMSO served as a suitable reference control. This enhancement in activity can be attributed to the chelation effect, which increases lipophilicity and facilitates the penetration of the complexes through the microbial cell membrane.

REFERENCE

1. Al Zoubi, W.; Al Mohanna, N. Spectrochim. Acta, Part A 2014, 132, 854–860.
2. Al Zoubi, W.; Al-Hamdani, A. A. S.; Kaseem, M. Appl. Organomet. Chem. 2016, 30, 810–818.
3. Al Zoubi, W.; Ko, Y. G. Appl. Organomet. Chem. 2017, 31, 1–8.
4. Al Zoubi, W.; Al-Hamdani, A. A. S.; Wifiantara, P.; Hamoodh, R. G.; Ko, Y. G. J. Phys. Org. Chem. 2017, https://doi.org/10.1002/poc.3707.
5. Al-Hamdani, A. A. S.; Balkhi, A. M.; Falah, A.; Shaker, S. A. J. Saudi Chem. Soc. 2016, 20, 487–495.
6. Sixt, T.; Kaim, W. Inorg. Chim. Acta 2000, 300, 762–770.
7. Ulusoy, M.; Birel, O.; Sahin, O.; Buyukgungor, O.; Cetinkaya, B. Polyhedron 2012, 38, 141–148.
8. Bose, D.; Banerjee, J.; Rahaman, S. K. H.; Mostafa, G.; Fun, H. K.; Bailey, W. R. D.; Zaworotko, M. J.; Ghosh, B. K. Polyhedron 2004, 23, 2045–2053.
9. El-Boraey, H. A. J. Therm. Anal. Calorim. 2005, 81(2), 339–345.
10. Al-Shirif, A. S. M.; Abdel-Fattah, H. M. J. Therm. Anal. Calorim. 2003, 71, 643–651.
11. Grivani, G.; Bruno, G.; Amiri Rudbari, H.; Khalaji, A. D. Inorg. Chem. Commun. 2012, 18, 15–18.
12. Khalaji, A. D.; Fejfarová, K.; Dušek, M. Acta Chim. Slov. 2010, 57, 257–262.
13. Khalaji, A. D.; Najafi Chermahini, A.; Fejfarová, K.; Dušek, M. Struct. Chem. 2010, 21(1), 153–159.
14. Al Zoubi, W.; Kandil, F.; Chebani, M. K. Spectrochim. Acta, Part A 2010, 79, 1909–1916.
15. Ashraf, M. A.; Mahmood, K.; Wajid, A. Int. Proc. Chem. Biol. Environ. Eng. 2011, 10, 1–6.
16. Cook, D. B. Handbook of Computational Quantum Chemistry; Oxford University Press: New York, 1998; pp 149–165.
17. Al Zoubi, W.; Kandil, F.; Chebani, M. K. Arab. J. Chem. 2016, 9(5), 626–634.
18. Coats, A. W.; Redfern, J. P. Nature 1964, 201, 68–69.
19. Al-Hamdani, A. A. S.; Hassan, Z. A. H. J. Chem. 2016, 13(3), 511–519.
20. Horovitz, H. H.; Metzger, G. Thermochim. Acta 1963, 159, 43–49.
21. Al Zoubi, W.; Ko, Y. G. J. Organomet. Chem. 2016, 82(1), 173–181.
22. Al Zoubi, W.; Kandil, F.; Chebani, M. K. Int. J. ChemTech Res. 2011, 3, 1612–1620.
23. Silverstein, R. M.; Webster, F. X. Spectrometric Identification of Organic Compounds, 7th ed.; John

Wiley & Sons: New York, 2005.
24. Nakamoto, K. Infrared and Raman Spectra of Inorganic and Coordination Compounds, 6th ed.; Wiley: New Jersey, 2009.
25. Al-Hamdani, A. A. S.; Balkhi, A. M.; Falah, A.; Shaker, S. A. J. Chil. Chem. Soc. 2015, 60(1), 2774–2780.
26. Al-Hamdani, A. A. S.; Ahmed, S. D.; Shaker, S. H.; Hassan, Z. A. H. Baghdad Sci. J. 2016, 13(2 Suppl.), 105–112.
27. Kunkeler, D.; Cornelissen, J.; Ree Dig, J. J. Am. Chem. Soc. 1996, 118, 2190–2196.
28. Keypour, H.; Wainwright, K.; Taylor, P. M. Iran. J. Chem. Soc. 2004, 1(1), 53–60.
29. Henryk, C.; Wojciech, K.; Florian, P. Int. J. Mol. Sci. 2001, 2, 1–9.
30. Al Zoubi, W.; Kandil, F.; Chebani, M. K. Arab. J. Chem. 2016, 9(4), 526–534.
31. Al-Hamdani, A. A. S.; Hammoda, R. G. Baghdad Sci. J. 2016, 13(4), 770–778.
32. Lever, A. B. P. Inorganic Electronic Spectroscopy; Elsevier: New York, 1968; pp 121–135.
33. Al-Hamdani, A. A. S. Dirasat Pure Sci. 2013, 39(1), 61–68.
34. Al-Hamdani, A. A. S.; Al Zoubi, W. Spectrochim. Acta, Part A 2015, 137, 75–83.
35. Al-Hamdani, A. A. S.; Balkhi, A. M.; Falah, A.; Shaker, S. A. Orient. J. Chem. 2011, 27(3), 825–833